Suppressing Defects Through Cooperation of Lewis Base and Lewis Acid for Perovskite Solar Cells with Efficiency Over 21% and Excellent Stability

Fei Zhang [1,2], Dongqin Bi [2], Norman Pellet [2], Chuanxiao Xiao [1], Zhen Li [1], Joseph J. Berry [1], Shaik Mohammed Zakeeruddin [2], Kai Zhu [1,*], Michael Grätzel [2,*]

[1] National Renewable Energy Laboratory, Golden, Colorado 80401, USA

[2] Laboratory of Photonics and Interfaces, Institute of Chemical Sciences and Engineering, École Polytechnique Fédérale de Lausanne (EPFL), Station 6 CH-1015, Lausanne, Switzerland

Correspondence and requests for materials should be addressed to K.Z. (email: kai.zhu@nrel.gov) or to M.G. (email: michael.graetzel@epfl.ch)

The commercial bis-PCBM mixed isomers as Lewis acid in the antisolvent and N-(4-bromophenyl)thiourea (BrPh-ThR) as Lewis base in the perovskite solution precursor were combined to investigate the cooperation of Lewis Base and Lewis Acid in this study. The combination of Lewis Base and Lewis Acid appears to synergistically passivate Pb^{2+} and PbX_3^- antisite defects, enlarge perovskite grain size, and improve the charge carrier separation as well as transportation within the perovskite film. In addition, this combination can also suppress moisture incursion and passivate pinholes generated in the hole-transporting layer. As a result, we obtained a power conversion efficiency (PCE) of 21.7% based on PSCs using bis-PCBM in the antisolvent along with BrPh-ThR in the precursor, compared with 19.3% for the control sample in the absence of bis-PCBM and BrPh-ThR, 20.4% with only the use of BrPh-ThR in the precursor, and 20.5% for just the addition of bis-PCBM in the antisolvent. The PCE of unsealed devices remained 93% in ambient air (10-20% RH) after 150 days at room temperature and dropped by 10% after 1500 h under continuous operation at 1-sun illumination in nitrogen with maximum power point tracking.

Perovskite solar cells (PSCs) have attracted significant attention due to their high power conversion efficiency (PCE) and potential low cost. In only eight years, their PCEs have rapidly increased from 3.8% to over 22%.[1–4] To date, many fabrication methods have been proposed and demonstrated to produce high-quality perovskite films.[5-10] Among them, the anti-solvent-assisted one-step method is a well proven effective strategy for obtaining excellent perovskite films with good uniformity and suitable grain sizes.[5,10]

In high-quality perovskite polycrystalline films, the bulk defect densities are often lower than the surface trap densities, contributing to the high PCE of PSCs.[11] Grain boundaries (GBs) as well as the surfaces in the perovskite thin films can significantly affect charge transport, recombination kinetics, device performance and stabilty.[12] In addition, owing to the ionic character of solution-processed perovskite semiconductors, the inherent ionic defects in the perovskite can also bring some undesired issues, such as hysteresis behavior, and device instability.[13,14] These and other results indicates, defect-induced electronic trap states at perovskite surface and GBs should be minimized for optimal device performance. Post-passivation treatment has been demonstrated to be an effective strategy to reduce the defect density in the perovskite films via bonding with uncoordinated halide or metal ions from perovskite crystals.[15,16] It was demonstrated that the treatment of perovskite crystals surfaces with Lewis base molecules such as thiophene, pyridine, thiourea, TDZDT, IT-M, 2-pyridylthiourea and DR3T could efficiently passivate the under-coordinated Pb atoms and thus improving the performance and stability.[15,17-23] Phenyl-C61-butyric acid methyl ester (PCBM) [24-26], Potassium iodide (KI)[27,28] and Zinc Chloride (ZnCl)[29], etc, as Lewis acid were also applied in the perovskite solution precursor to improve film formation and increase environmental stability. Realizing stability at these efficiencies is critical to advancing PSC and the degradation in perovskite based solar cells can stem from a myriad of sources within the device.[30] The deleterious impact of water/oxygen molecules intrusion into the perovskite active

layer are well documented but can be relieved via engineering of the interfaces within the device stack.[31] Moreover, recent studies show that moisture-sensitive defects, likely prevalent at grain boundaries play, an important role in triggering the moisture-induced degradation process. The impact of defect passivation within the active layer, by combining the Lewis acid and Lewis base at the same time to achieve a high PCE, on stability of power production or even under light soaking have not been examined.

In this paper, we applied the commercial bis-PCBM mixed isomers as Lewis acid in the anti-solvent and N-(4-bromophenyl)thiourea (BrPh-ThR) as Lewis base in the perovskite solution precursor to investigate the cooperation of Lewis Base and Lewis Acid. Lewis acids can accept an electron from the negative-charged Pb-I antisite defects PbI_3^- or under-coordinated halide ions and thus passivate the halide-induced deep traps [32-34]. Lewis bases, usually function as the electron donors, which can bind to the positively charged under-coordinated Pb^{2+} ions [17-22]. However, most of these passivation molecules should only passivate one type of defect. The results show that the combination of Lewis Base and Lewis Acid can passivate both defects, enlarge perovskite grain size, and improve charge carrier separation and transportation. Thus, compared with 19.3% for control a PCE of 20.4% is obtained for only using BrPh-ThR in the precursor, 20.5% for only using bis-PCBM in the antisolvent and a PCE of 21.7%, when combining the bis-PCBM laced antisolvent along with BrPh-ThR in the precursor. Importantly, this PCE remained the 93% and 90% of the initial value after 150 days in ambient air (10-20% RH) at room temperature and after 1500 h under continuous full sun illumination at maximum power point tracking, respectively.

Results

Mechanistic study of suppressing defects. A schematic illustration of the Lewis acid and Lewis base-assisted growth process for the perovskite layer is shown in **Figure 1**. The mixed cation perovskite $[(FAI)_{0.81}(PbI_2)_{0.85}(MABr)_{0.15}(PbBr_2)_{0.15}]$ precursor is prepared from a solution of formamidinium iodide (FAI), PbI_2, methylammonium bromide (MABr) and $PbBr_2$

in a mixed solvent of dimethyl formamide (DMF) and dimethyl sulfoxide (DMSO) with 1.35M Pb^{2+}(PbI_2 and $PbBr_2$) and 0.6 mg/ml BrPh-ThR, then are spin-coated on mesoporous TiO_2. During the last 15 s of second spin coating step, 110 mL of bis-PCBM containing chlorobenzene (CB) was dropped onto the above film to promote the formation of an intermediate phase and the cooperation of Lewis base BrPh-ThR. BrPh-ThR as an S-donor has a stronger ability coordinating with PbI_2 to gain the flexibility of tuning the coordination strength and passivate the Pb^{2+} defects. The bis-PCBM can passivates the key PbX_3^- antisite defects and also template the nucleation of perovskite.

In order to examine this hypothesis, we performed the liquid-state ^1H nuclear magnetic resonance (^1H NMR) spectroscopy and the results are shown in **Figure S1-S2**. When adding some PbI_2 in the solution, the signals of -NH- and $-NH_2$ in the BrPh-ThR and $-CH_3$ in bis-PCBM were all shifted, indicating the formation of -C=S-•Pb and -C=O-R-C=O-•Pb, respectively. The presence of $[(FAI)_{0.81}(PbI_2)_{0.85}(MABr)_{0.15}(PbBr_2)_{0.15}]$ induces a stronger chemical shift than that in the PbI_2 solution, indicating the possible formation of MA(FA)I(Br)•Br-C=S-•Pb and MA(FA)I(Br)•-C=O-R-C=O-•Pb, respectively. When we added BrPh-ThR and bis-PCBM in the perovskite solution at the same time, the chemical shift was larger than that using either BrPh-ThR or bis-PCBM, indicating the synergistic effect from the cooperation of these two compounds.

To get insight into the surface defect passivation effect of BrPh-ThR and bis-PCBM for perovskite films, we performed photoluminescence (PL) and time-resolved PL (TRPL) decay measurements for the corresponding samples on a glass substrate. When compared with the pristine perovskite film, the normalized steady-state PL spectra, shown in **Figure 2a**, indicates blue shifting of 4 nm, 5 nm and 7 nm for BrPh-ThR-containing, bis-PCBM-containing, and BrPh-ThR along with bis-PCBM-containing perovskite layers, respectively. Such blue shifting and line narrowing is attributed to decrease of spontaneous radiative recombination between trap states, which could account for the increased V_{oc} and FF.[35] TRPL decay data are presented

in **Figure 2b** and fitted to the equation **S3** derived in the supporting information [36]. This equation reduced to an exponential rate law at longer times. Linear fits of the curves in the time domain are excellent as shown in **Figure S3** and yield the lifetimes for nonradiative carrier recombination listed in **Table S1**. The lifetimes follow the order, BrPh-ThR along with bis-PCBM-containing film > bis-PCBM-containing film > BrPh-ThR-containing film > pristine control perovskite film. This further confirms that the synergistic effect of using both Lewis base (BrPh-ThR) and Lewis acid (bis-PCBM) on reducing defect density in perovskite films, which again is consistent with the higher V_{oc} and FF of the corresponding PSC. [37]

To assess the defect density and charge transport, we conducted the space charge limited current (SCLC) measurement of the corresponding perovskite films and the I–V characteristics of the different devices are shown in **Figure S4** and corresponding data are summarized in **Figure 2c**. Typical three regions of J–V curves were observed in both devices in a log–log representation. In the low-bias region, the current density is proportional to voltage, which reflects an Ohmic contact with electrode. With increasing bias, the current density increased abruptly corresponding to a trap-filled limit (TFL) current.[38] We calculated the trap-state density (N_t) using the trap-filled limit voltage equation $N_t = 2\varepsilon\varepsilon_0 V_{TFL}/qd^2$,where ε_0 is is the dielectric constant of vacuum permittivity, ε is the relative dielectric constant of perovskite, q is the elementary charge, d is the thickness of the perovskite film, and V_{TFL} is determined from the *J–V* curve.[39] Although the presumptions of this analysis maybe questioned in the context of the halide perovskite materials it none the less provides a relative measure of the trap densities and we can estimate the trap densities for corresponding perovskite films. The defect density of BrPh-ThR along with bis-PCBM-containing perovskite film is substantially lower than the other three films, which is consistent with the PL/TRPL results as well as the higher V_{oc} and FF in solar cells. We also calculated the mobility of the different perovskite films using the equation $J = 9\varepsilon\varepsilon_0\mu V^2/8d^2$. The mobility values were estimated to be 9.26 $cm^2\ V^{-1}\ S^{-1}$, 13.71 $cm^2\ V^{-1}\ S^{-1}$, 16.52 $cm^2\ V^{-1}\ S^{-1}$and 20.91 $cm^2\ V^{-1}\ S^{-1}$ for pristine, BrPh-ThR-containing, bis-

PCBM-containing, and BrPh-ThR along with bis-PCBM-containing perovskite films, respectively. The improved mobility and longer lifetime are consistent with the higher J_{sc} of the corresponding PSCs.[40]

It is generally established that localized defects in the perovskite GBs and grain interiors (GIs) may serve as recombination centers, which are detrimental to PSC performance. Moreover, these localized defects may result in inefficient photo carrier separation and transportation, leading to poor conducting properties of perovskite films.[22,41] We carried out conductive atomic force microscopy (c-AFM) to investigate conducting properties of corresponding perovskite films. As shown in **Figure S5c-f**, the control sample showed comparatively low current signal, which indicates poor electrical conductivity of perovskite films. In contrast, the perovskite films with BrPh-ThR and bis-PCBM present a significantly increased current signal at both the GBs and GIs, which suggests that surface trap states can be efficiently passivated with BrPh-ThR and bis-PCBM, which correlates well with decreased trap density (SCLC) and improved carrier lifetime (TRPL). It is worth noting that the GBs show brighter contrast than GIs, revealing relatively higher current flow associated with more efficient charge transfer, which is in good agreement with the previous report.[42]

The X-ray diffraction (XRD) measurements were performed to study the crystalline structure of perovskite films on m-TiO_2/c-TiO_2/FTO substrates (**Figure 2d**). The XRD patterns depict a set of characteristic peaks, which are indicative of the tetragonal perovskite structure. XRD spectra exhibit similar, strong, and sharp perovskite characteristic peaks. The intensity of bis-PCBM and BrPh-ThR containing perovskite film at (110) peak becomes stronger and the full width at half-maximum (FWHM) decreased (**Figure S6a,b**) when compared with the pristine perovskite film, bis-PCBM-containing and BrPh-ThR-containing perovskite films, which also shows that bis-PCBM and BrPh-ThR can improve the crystallization of perovskite and /or more preferred (110) orientation. We attribute the improved crystallization process to

the templating effect of bis-PCBM and BrPh-ThR on the crystal growth. We ascribe the high-quality crystallization as one of the main factors for improved device performance.[43]

Scanning electron microscopy (SEM) images of the corresponding perovskite films deposited on m-TiO_2/c-TiO_2/FTO substrate are presented in **Figure 3**. As illustrated from the top-view SEM, the change in morphology is consistent with an increase in grain size of the perovskite film with the use of either BrPh-ThR or bis-PCBM and directs most of GBs to assume a perpendicular orientation to the substrate. After the use of both, the grain size becomes larger and thus reduced the GB density. Hence, BrPh-ThR along with bis-PCBM appears to uniformly promote heterogeneous nucleation over the perovskite precursor film, improving the grain size and facilitating perovskite growth with preferred direction. The morphology of the perovskite thin films with and without BrPh-ThR and bis-PCBM were further studied by AFM, as shown in **Figure S5a, b**. It can be found that with BrPh-ThR and bis-PCBM, the root mean squared (rms) roughness of the perovskite film became smaller than that of the control films. The result shows that with the cooperation of BrPh-ThR and bis-PCBM, the perovskite thin film can be smoother and more uniform, which are beneficial for effective charge transport and higher photovoltaic performance.[44] **Figure S6b** presents the absorption spectra of the corresponding films. Compared with the pristine control perovskite film, obvious absorption enhancement is observed in almost the entire visible-light region for perovskite films using BrPh-ThR and/or bis-PCBM; this enhancement is likely originated from the contribution of their impact on larger grain size and more uniform crystal formation of perovskite. These results could contribute to the much enhanced short-circuit current density (J_{sc}) in the corresponding PSCs.

Figure 4a shows contact-angle measurements of a deionized water droplet with the corresponding perovskite film. The derived contact angles are 57.6°, 68.1°, 69.2° and 77.8° for pristine control, BrPh-ThR-containing, bis-PCBM-containing and the BrPh-ThR along with

bis-PCBM-containing film respectively. This trend reflects a strong increase in hydrophobicity of the perovskite upon incorporation of the BrPh-ThR along with bis-PCBM resulting in its greatly enhanced stability against degradation in humid air. We exposed unsealed films of pristine, BrPh-ThR, bis-PCBM, and BrPh-ThR along with bis-PCBM-containing perovskite thin films to ambient environment of 45% relative humidity, and periodically recorded their X-ray diffraction patterns as shown in **Figure 4b**. The decomposition of perovskite in moist air is known to lead to the formation of a PbI_2 phase. The ratio of PbI_2 ($2\theta = 12.5°$) to perovskite ($2\theta = 13.8°$) of pristine control perovskite increases faster than that of BrPh-ThR-containing, bis-PCBM-containing, and BrPh-ThR along with bis-PCBM-containing perovskite film after 30 days. The BrPh-ThR along with bis-PCBM -containing perovskite film turned out to be the most stable one in this test environment, indicating the stability is improved after the Lewis acid and Lewis base cooperation. The enhanced stability of the BrPh-ThR along with bis-PCBM -containing perovskite film can also be seen from the **Figure 4c**, which shows that the color of the BrPh-ThR along with bis-PCBM -containing perovskite films remain persistent; whereas, those of the bis-PCBM-containing and BrPh-ThR-containing perovskite films change a little and pristine control perovskite film almost turned to yellow.

Photovoltaic devices and performance. The cell architecture in this study adopted the traditional mesoporous structure with a full device stack Au/spiroOMeTAD/ perovskite /mesoporous TiO_2/compact TiO_2/FTO. The typical current density-voltage (J–V) curves of pristine, BrPh-ThR-containing, bis-PCBM-containing, and BrPh-ThR along with bis-PCBM-containing perovskite films layer-based PSCs under AM 1.5 G illumination with the light intensity of 100 mW cm^{-2} are shown in **Figure 5a-d** and corresponding data were summarized in **Table S2**. The control device delivers a champion PCE of 19.3%, with V_{oc} of 1.10V, J_{sc} of 23.13 mA cm^{-2}, and fill factor (FF) of 0.73, which is consistent with previous report.[45] In contrast, BrPh-ThR-containing, bis-PCBM-containing and BrPh-ThR along with bis-PCBM-

containing perovskite-based devices displayed better performance with PCE of 20.4 %, 20.5% and 21.7%. As previously reported,[19,24] Lewis acid bis-PCBM or Lewis base thiourea plays a critical role in improving the quality of the active layer with large grains and fewer grain boundaries, which result in obviously enhanced J_{sc} and FF. This study shows that combination of Lewis base and Lewis acid gives a substantially greater performance enhancement. We ascribed the improvement in J_{sc} with Lewis base BrPh-ThR along with Lewis acid bis-PCBM-containing to be mainly due to higher conductivity [**Figure S5**], higher mobility [**Figure 2c**, **Table S2**], lower defect concentration and no obvious boundaries. The hysteresis loss calculated from equation $\text{Hysteresis loss } \% = \frac{P_{forward} - P_{backward}}{P_{forward}}$ of devices based on pristine, BrPh-ThR-containing, bis-PCBM-containing, and BrPh-ThR along with bis-PCBM-containing perovskite films are 2.08%, 0.49%, 0.48% and 0.46%. The origination of hysteresis in PSCs is reported to be due to the trap state of charge carriers, ion charge carriers, ion migration and ferroelectricity, which are related to grain size and defect density.[46,47] The combination of Lewis base and Lewis acid-containing perovskite films has the largest grain size, lowest defect density, highest carrier mobility and highest conductivity resulting in the most negligible hysteresis. The stabilized power outputs from devices based on pristine perovskite, BrPh-ThR-containing, bis-PCBM-containing, and BrPh-ThR along with bis-PCBM-containing perovskite layer are 19.1 %, 20.3%, 20.4% and 21.5% respectively (**Figure 5e**), which are consistent with the obtained PCEs.

The incident photon-to-electron conversion efficiency (IPCE) spectra of the cells based on the corresponding perovskite layers are presented in **Figure 5f**. The integrated current densities estimated from the IPCE spectra are: 21.6 mA cm^{-2}, 22.1 mA cm^{-2}, 22.2 mA cm^{-2} and 22.7 mA cm^{-2} for pristine perovskite, BrPh-ThR-containing, bis-PCBM-containing, and BrPh-ThR along with bis-PCBM-containing perovskite layer-based solar cells, respectively. These are in good agreement with the J_{sc} values obtained from the *J-V* curves. The reproducibility of the device

performance was evaluated by characterizing about 20 cells. Histograms of the PCE parameters of these devices (**Figures 6a-d**) indicate excellent reproducibility.

Operational stability of perovskite solar cells. The long-term stability of PSCs is a challenging issue and can be significantly impacted by choice of device architecture that will modulate the role of atmosphere.[48] The initial stability data of PSC is shown in **Figure 6e,f** and **S8** for tests of the corresponding PSCs without encapsulation under an ambient environment of 10-20% relatively humidity and under continuous full sun illumination at the maximum power point tracking in a nitrogen atmosphere at room temperature. These studies provide clear evidence that the use of bis-PCBM, and BrPh-ThR do not introduce an additional instability for the active layers in this device architecture and the combination of Lewis base BrPh-ThR and Lewis acid bis-PCBM-containing perovskite based device presents a further and very substantial increase in stability over the control. For example, **Figure 6e** shows the combination of Lewis base BrPh-ThR and Lewis acid bis-PCBM -containing perovskite-based device maintained 93.2% of its initial PCE after 150 days without encapsulation; whereas under the same conditions the measured PCEs decreased to 71.7%, 67.6% and 32.6% of their initial values in the bis-PCBM-containing, BrPh-ThR-containing, and pristine control perovskite based solar cells, respectively. Stability data presented in **Figure 6f** indicates that there is only a 10% efficiency drop after 1500 h continuous 1-sun illumination in a nitrogen atmosphere with maximum power point tracking for combination of Lewis base BrPh-ThR and Lewis acid bis-PCBM -containing PSC. At the same time, the PCEs decreased by 23.6%, 32.1% and 86.1% of their initial values in the bis-PCBM-containing, BrPh-ThR-containing and pristine control perovskite based solar cells, respectively. The improved efficiency without compromise in stability for this device architectures indicates the combination of Lewis base BrPh-ThR and Lewis acid bis-PCBM-containing perovskite can further enhance PSC stability and technological viability. This is consistent with the ability of this treatment to limit defects

enhanced interaction between organic species (MA and FA) impacting the $[PbX_6]^{4-}$(X: Br and I) octahedral as well as limiting the other moisture-sensitive defects (Pb^{2+}). The structural, morphological and hydrophobicity that result the defect passivation also appear to result in practical improvements which aid stability (fewer pinholes in the spiro-OMeTAD layer (**Figure S9**), larger grain size, less pronounced boundaries etc) that should translate improvements in other device architectures.[22,45,46,49,50]

Discussion

In conclusion, we have demonstrated PSCs with simultaneously improved device performance and stability by combination of Lewis base BrPh-ThR in the perovskite solution precursor and Lewis acid bis-PCBM in the antisolvent during the device fabrication for the first time. The Lewis base BrPh-ThR and Lewis acid bis-PCBM can enhance resistance to moisture incursion, passivate the defects in the absorber layer, and suppress pinholes generated in the HTM layer. The combination of Lewis base BrPh-ThR and Lewis acid bis-PCBM positively enhances the crystallization, mobility and conductivity of perovskites. These beneficially factors lead to much improved device performance and stability. This promising approach provides a simple route for the fabrication of highly efficient and stable bulk heterojunction PSCs.

Acknowledgements:

We thank Mr. Linfeng Pan from LSPM for Hall Effect test, Mr. Hongwei Zhu from Tianjin University for ^{1}H NMR and SCLC test, and Dr. Rothenberger Guido from LPI for the TRPL analysis. M.G. and S.M.Z. are grateful to the Swiss National Science Foundation for the joint project IZLRZ2_164061 under the Scientific & Technological Cooperation Program Switzerland-Russia, the European Union's Horizon 2020 research and innovation program (under grant agreement No 687008, GOTSolar) and the King Abdulaziz City for Science and

Technology (KACST) for financial support. F.Z., K.Z. and J.J.B. were supported by the US Department of Energy under Contract No. DE-AC36-08GO28308 with Alliance for Sustainable Energy, Limited Liability Company (LLC), the Manager and Operator of the National Renewable Energy Laboratory. The authors acknowledge support from the hybrid perovskite solar cell program of the National Center for Photovoltaics, funded by the US Department of Energy, Office of Energy Efficiency and Renewable Energy, Solar Energy Technologies Office.

Author contributions

F.Z. designed the experiment, carried out the experimental study on device fabrication and performed basic characterization. F.Z. and D.Q.B performed the PL and contact angles test. N.M, D.Q.B and F.Z performed the stability test. C.X.X performed the AFM test. Z.L and F.Z performed SEM and XRD measurements. Z.F wrote the first draft of the paper. All authors made a substantial contribution to the discussion of the content and reviewed and edited the manuscript before submission. S.M.Z. coordinated the research, whereas K.Z and M.G. supervised the project.

Competing interests

The authors declare no competing interests.

References

[1] Saliba, M. et al. Incorporation of rubidium cations into perovskite solar cells improves photovoltaic performance. *Science* **354**, 206-209 (2016).

[2] NREL. Best Research-Cell Efficiencies, http://www.nrel.gov/ncpv/images/effi ciency_chart.jpg . (**May 2018**)

[3] Shin, S. S. et al. Colloidally prepared La-doped $BaSnO_3$ electrodes for efficient, photostable perovskite solar cells. *Science* **356**,167-171(2017).

[4] Yang, W. S. et al. High-performance photovoltaic perovskite layers fabricated through intramolecular exchange. *Science*. **348**, 1234-1237 (2015).

[5] Bi, D. Q. et al. Polymer-templated nucleation and crystal growth of perovskite films for solar cells with efficiency greater than 21%. *Nat. Energy*. **1**, 16142(2016).

[6] Chen, Q. et al. Planar Heterojunction Perovskite Solar Cells via Vapor-Assisted Solution Process. *J. Am. Chem. Soc.* **136**, 622-655(2013).

[7] Li, X. et al. A vacuum flash-assisted solution process for high-efficiency large-area perovskite solar cells. *Science* **353**, 58-62(2016).

[8] Xiao, Z. et al. Efficient, high yield perovskite photovoltaic devices grown by inter diffusion of solution-processed precursor stacking layers. *Energy Environ. Sci.* **7**, 2619-2623(2014).

[9] Liu, M. Johnston, M. B. Snaith, H. J. Efficient planar heterojunction perovskite solar cells by vapour deposition. *Nature* **501**, 395-398(2013).

[10] Xiao, M. et al. A fast deposition-crystallization procedure for highly efficient lead iodide perovskite thin-film solar cells. *Angew Chem Int Ed*. **53**, 9898-9903 (2014).

[11] Xing, G. et al. Low-temperature solution-processed wavelength-tunable perovskites for lasing. *Nat. Mater*. **13**, 476-480(2014).

[12] Christians, J. A. et al. Tailored interfaces of unencapsulated perovskite solar cells for >1,000 hour operational stability. *Nat. Energy*. **3**, 68-74(2018).

[13] Berhe, T. A. et al. Organometal halide perovskite solar cells: degradation and stability. *Energy Environ. Sci.* **9**, 323-356(2016).

[14] Tiep, H. Ku, Z. Fan, H. J. Recent Advances in Improving the Stability of Perovskite Solar Cells. *Adv. Energy Mater.* **6**, 1501420(2016).

[15] Noel, N. K. et al. Enhanced Photoluminescence and Solar Cell Performance via Lewis Base Passivation of Organic-Inorganic Lead Halide Perovskites. *ACS Nano* **8**, 9815-9821(2014).

[16] Lin, Y. et al. π−Conjugated Lewis Base: Efficient Trap-Passivation and Charge-Extraction for Hybrid Perovskite Solar Cells. *Adv. Mater*. **29**, 1604545(2017).

[17] Fei, C. B., Li, B., Zhang, R., Fu, H.Y., Tian, J. J., Cao, G. Z., Highly Efficient and Stable Perovskite Solar Cells Based on Monolithically Grained $CH_3NH_3PbI_3$ Film. *Adv. Energy Mater.* **7**, 1602017(2017).

[18] Lee, J., Kim, H., Park, N. G. Lewis Acid-Base Adduct Approach for High Efficiency Perovskite Solar Cells. *Accounts of Chemical Research*, **49**, 311-319(2016).

[19] Zhu, L. F. et al. Investigation on the role of Lewis bases in the ripening process of perovskite films for highly efficient perovskite solar cells. *J. Mater. Chem. A*. **5**, 20874–20881(2017).

[20] Zhu, H., Zhang, F. Xiao, Y., Wang, S., Li, X., Suppressing defects through thiadiazole derivatives that modulate $CH_3NH_3PbI_3$ crystal growth for highly stable perovskite solar cells under dark conditions. *J. Mater. Chem. A*. **6**, 4971-4980(2018).

[21] Niu, T. Q. et al. Stable High-Performance Perovskite Solar Cells via Grain Boundary Passivation. *Adv. Mater*. **30**, 1706576(2018).

[22] Yang, G., Qin, P. L., Fang, G. J., Li, G. A Lewis Base-Assisted Passivation Strategy Towards Highly Efficient and Stable Perovskite Solar Cells. *Sol. RRL*. 1800055(2018).

[23] Sun, M., Zhang, F., Liu, H., Li, X., Xiao, Y., Wang, S. Tuning the crystal growth of perovskite thin-films by adding the 2-pyridylthiourea additive for highly efficient and stable solar cells prepared in ambient air. *J. Mater. Chem. A*. **5**, 13448–1345(2017).

[24] Zhang, F. et al. Isomer-Pure Bis-PCBM-Assisted Crystal Engineering of Perovskite Solar Cells Showing Excellent Efficiency and Stability. *Adv. Mater.* **29**, 1606806(2017).

[25] Wang, K. Liu, C., Du, P. C., Zheng, J., Gong, X. Bulk heterojunction perovskite hybrid solar cells with large fill factor. *Energy Environ. Sci.* **8**, 1245-1255(2015).

[26] Chiang, C. H., Wu, C. G. Bulk heterojunction perovskite-PCBM solar cells with high fill factor. *Nat. Photonics.* **10**, 196-200(2016).

[27] Abdi-Jalebi, M. et al. Maximizing and stabilizing luminescence from halide perovskites with potassium passivation. *Nature* **555**, 497–501(2018).

[28] Tang, Z. G.et al. Hysteresis-free perovskite solar cells made of potassium-doped organometal halide perovskite. *Sci. Reports*, **7**, 12183(2017).

[29] Jin, J. J. et al. Enhanced Performance of Perovskite Solar Cells with Zinc Chloride Additives. *ACS Appl. Mater. Interfaces*, **9**, 42875-42882(2017).

[30] Domanski, K., Alharbi, E. A., Hagfeldt, A., Grätzel, M., Tress, W. Systematic investigation of the impact of operation conditions on the degradation behaviour of perovskite solar cells. *Nat. Energy*. **3**, 61–67(2018).

[31] Sanehira, E. M. et al. Influence of Electrode Interfaces on the Stability of Perovskite Solar Cells: Reduced Degradation Using MoO_x/Al for Hole Collection. *ACS Energy Lett.* **1**, 38-45(2016).

[32] Zheng, X. P. et al. Defect passivation in hybrid perovskite solar cells using quaternary ammonium halide anions and cations. *Nat. Energy*. **2**, 17102(2017).

[33] Xu, J. et al. Perovskite–fullerene hybrid materials suppress hysteresis in planar diodes. *Nat. Commun*. **6**, 7081(2015).

[34] Abate, A.et al. Supramolecular Halogen Bond Passivation of Organic–Inorganic Halide Perovskite Solar Cells. *Nano Lett*. **14**, 3247-3254(2014).

[35] Dong, Q. F. et al. Electron-hole diffusion lengths > 175 μm in solution-grown $CH_3NH_3PbI_3$ single crystals. *Science,* **347**, 967-970(2015).

[36] Tavakoli, M. M., Bi, D. Q., Pan, L. F., Hagfeldt, A., Zakeeruddin, S. M., Grätzel, M. Adamantanes Enhance the Photovoltaic Performance and Operational Stability of Perovskite Solar Cells by Effective Mitigation of Interfacial Defect States. *Adv. Energy Mater*. 1800275 (2018).

[37] Wu, Y. Z. et al. Perovskite solar cells with 18.21% efficiency and area over 1 cm^2 fabricated by heterojunction engineering. *Nature Energy*, **1**, 16148(2016).

[38] Jiang, L. L. et al. Passivated Perovskite Crystallization via g-C3N4 for High-Performance Solar Cells. *Adv. Funct. Mater.* **28**, 1705875(2018).

[39] Liu, Z. H. et al. Chemical Reduction of Intrinsic Defects in Thicker Heterojunction Planar Perovskite Solar Cells. *Adv. Mater.* **29**, 1606774(2017).

[40] Zhang, X. et al. Stable high efficiency two-dimensional perovskite solar cells via cesium doping. *Energy Environ. Sci.*, **10**, 2095–2102(2017).

[41] Lee, J. K. et al. A Bifunctional Lewis Base Additive for Microscopic Homogeneity in Perovskite Solar Cells. *Chem*, **3**, 290–302(2017).

[42] Son, D.-Y. et al. Self-formed grain boundary healing layer for highly efficient $CH_3NH_3PbI_3$ perovskite solar cells. *Nat Energy*, **1**, 16081(2016).

[43] Wang, Z. K. et al. Induced Crystallization of Perovskites by a Perylene Underlayer for High-Performance Solar Cells. *ACS Nano*. **10**, 5479(2016).

[44] Li, C., Sleppy, J., Dhasmana, N., Soliman, M., Tetardd, L., Thomas, J. A PCBM-assisted perovskite growth process to fabricate high efficiency semitransparent solar cells. *J. Mater. Chem. A*, **4**, 11648–11655(2016).

[45] Bi, D. Q. et al. Efficient luminescent solar cells based on tailored mixed-cation perovskites. *Sci. Adv.* **2**, e1501170 (2016).

[46] Chu, Z. D. et al. Impact of grain boundaries on efficiency and stability of organic-inorganic trihalide perovskites. *Nature Communications*, **8**, 2230(2017).

[47] Yuan, Y., Huang, J. S., Ion Migration in Organometal Trihalide Perovskite and Its Impact on Photovoltaic Efficiency and Stability. *Acc.Chem. Res*. **49**, 286-293(2016).

[48] Li, X. et al. Improved performance and stability of perovskite solar cells by crystal crosslinking with alkylphosphonic acid ω-ammonium chlorides. *Nat. Chem.* **7**, 703-711(2015).

[49] Back, H. et al. Achieving long-term stable perovskite solar cells via ion neutralization. *Energy Environ. Sci.* **9**, 1258-1263(2016).

[50] Zhang, F. et al. A Novel Dopant-Free Triphenylamine Based Molecular "Butterfly" Hole-Transport Material for Highly Efficient and Stable Perovskite Solar Cells. *Adv. Energy Mater*. **6**, 1600401(2016).

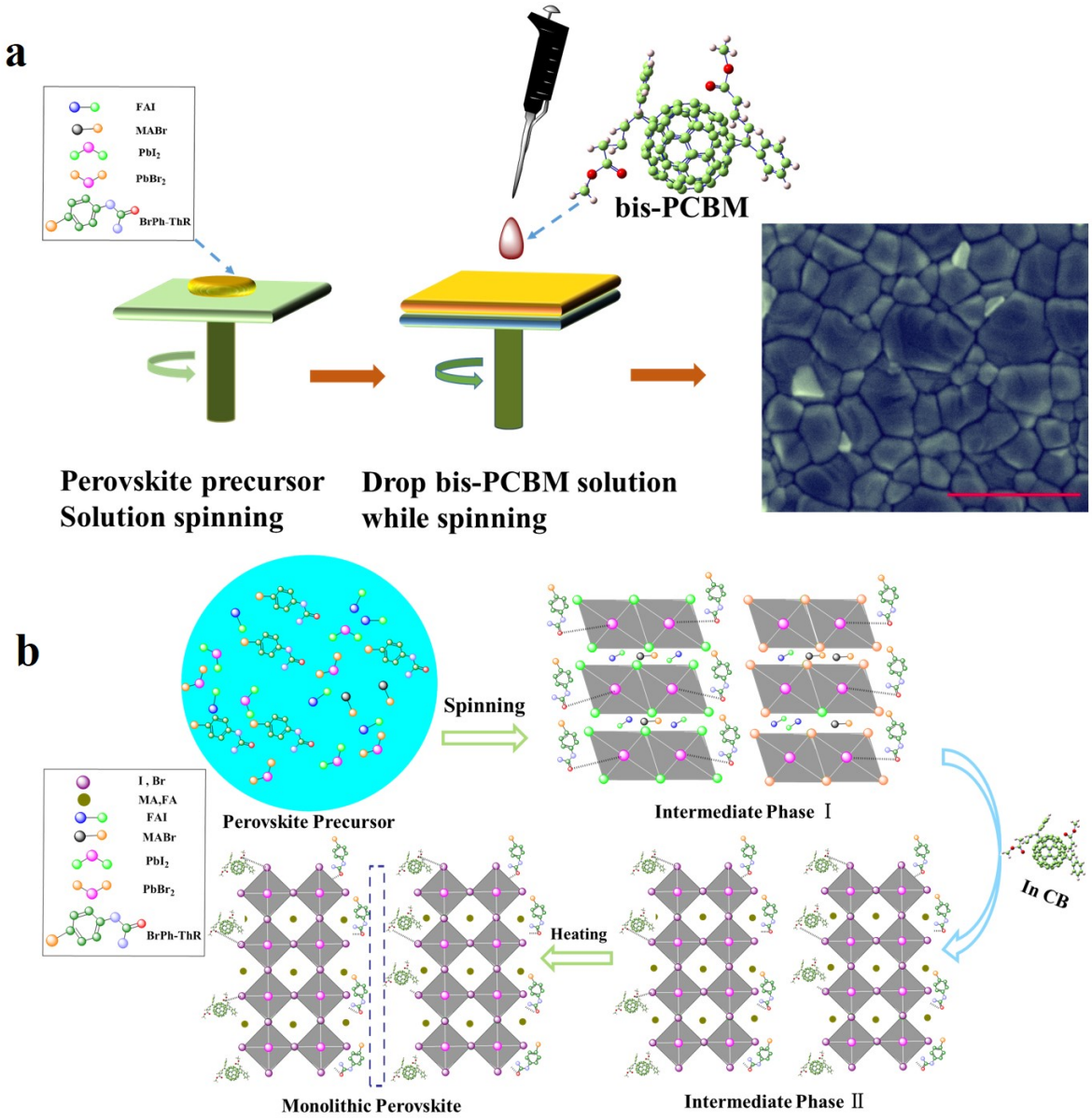

Figure 1 (a) Schematic diagram of antisolvent process; (b) Schematic reaction process of perovskite growth resulting in combination of Lewis base BrPh-ThR in the perovskite solution precursor and Lewis acid bis-PCBM in the antisolvent process.

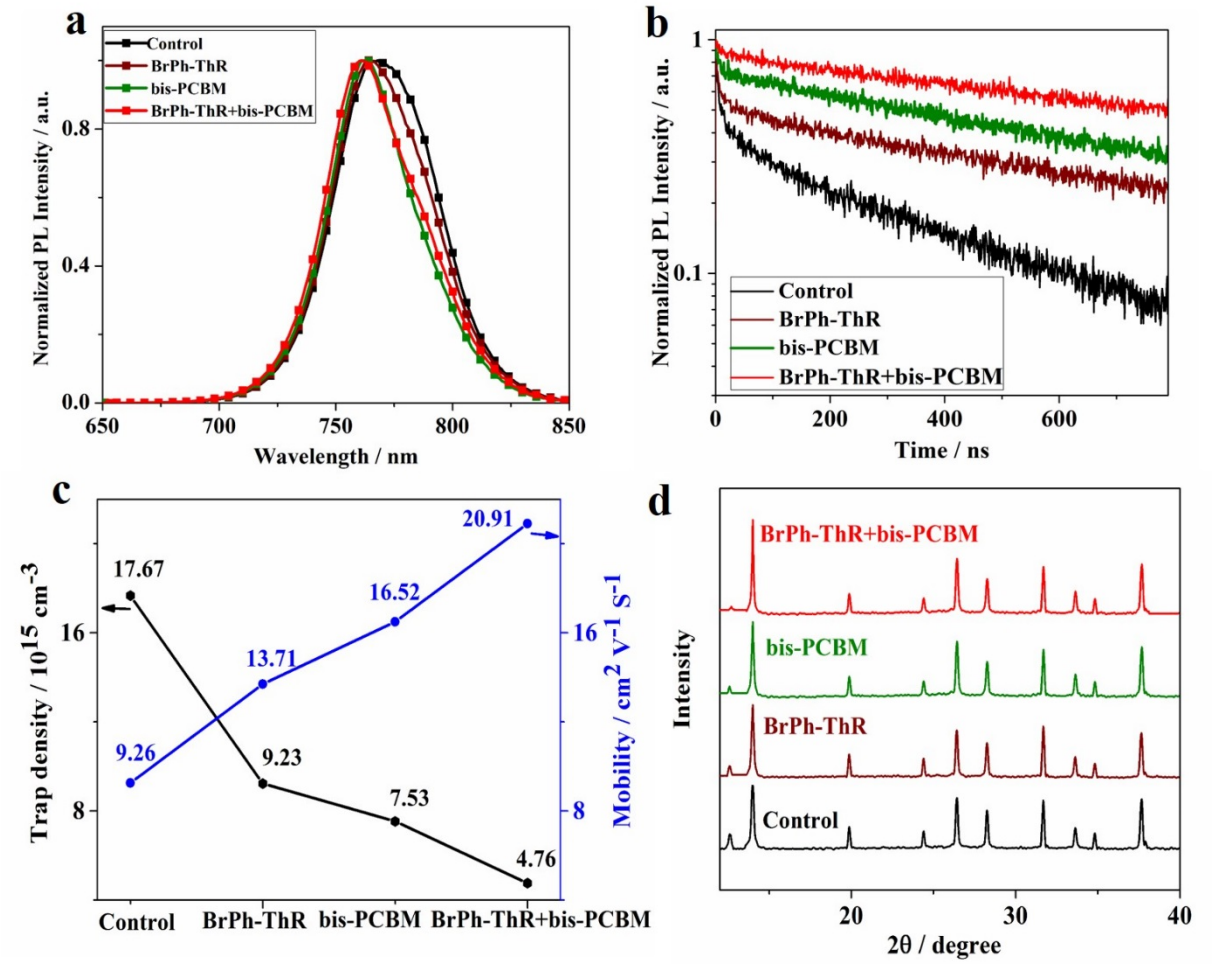

Figure 2 a) PL spectra, b) TRPL spectra of corresponding films on glass substrate; (c)Trap density and mobility data of corresponding films obtained from SCLC method; (d)XRD patterns of corresponding films on meso-TiO_2/compact TiO_2/FTO substrate.

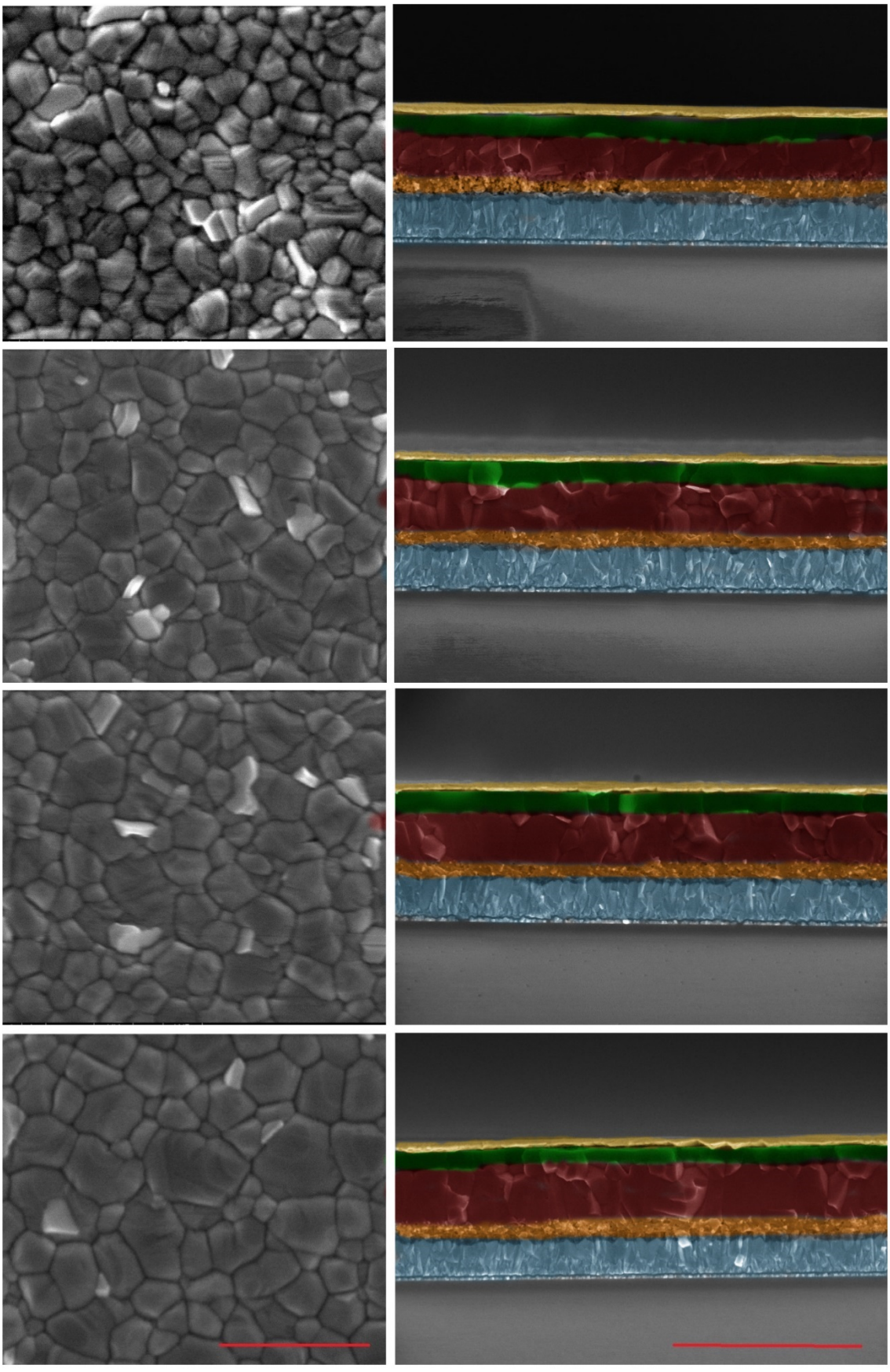

Figure 3 Scanning electron microscopy images. Top (left, the scale is 1μm) SEM of corresponding perovskite films and cross sectional (right, the sacle is 2 μm) SEM of corresponding perovskite devices. 1, Control; 2, BrPh-ThR; 3, bis-PCBM;4, BrPh-ThR+ bis-PCBM.

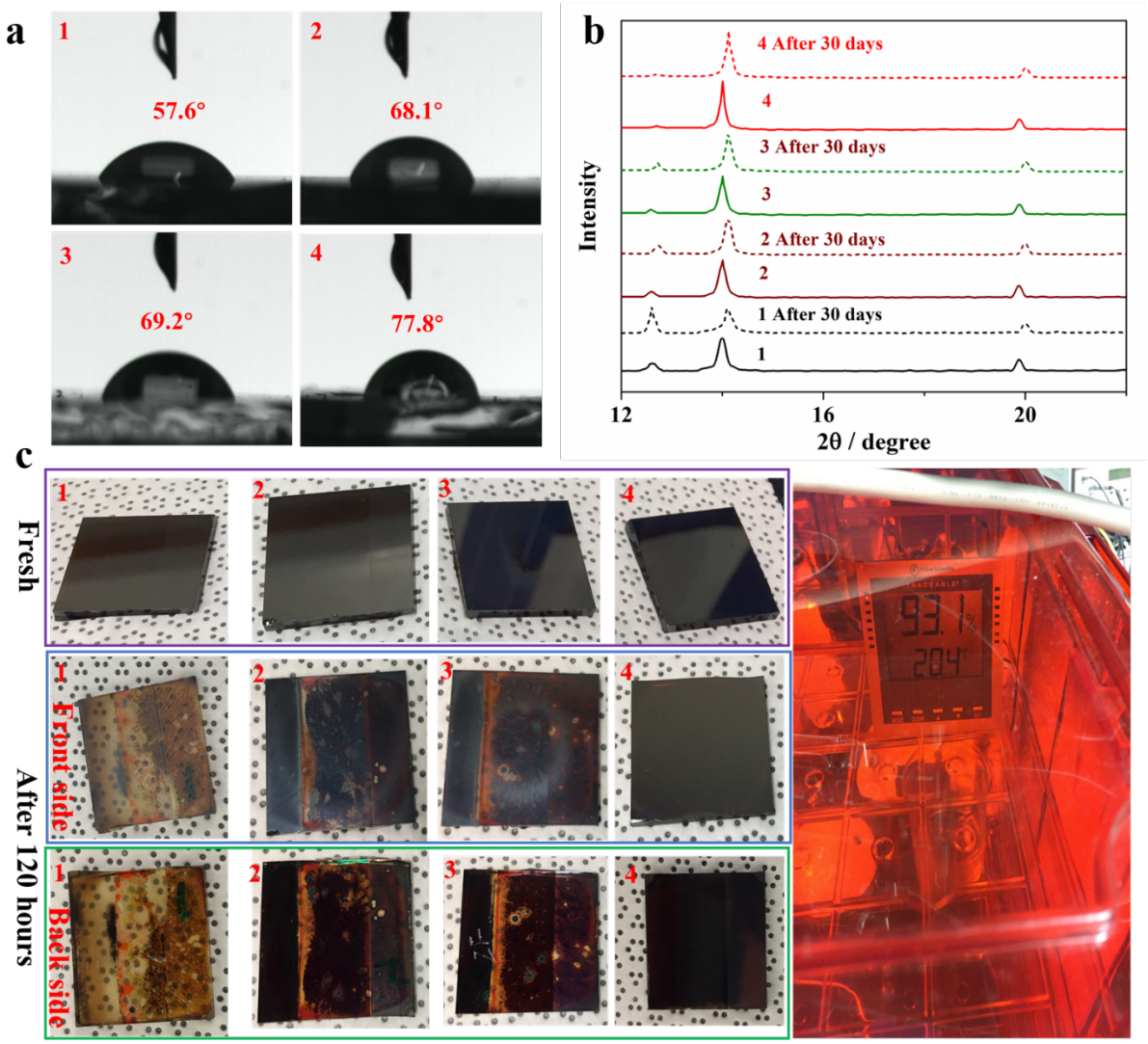

Figure 4 a) The contact angles between corresponding perovskite films and water; b) XRD patterns of corresponding films on meso-TiO_2/compact TiO_2/FTO substrate, which were exposed to ambient 45% relative humidity before and after 30 days; c) The pictures of the corresponding films before and after aging to ambient 93% relative humidity by 120 hours, the first line are fresh films and the second and the third line are frontside and backside of aging films, respectively. 1, Control; 2, BrPh-ThR; 3, bis-PCBM; 4, BrPh-ThR+ bis-PCBM.

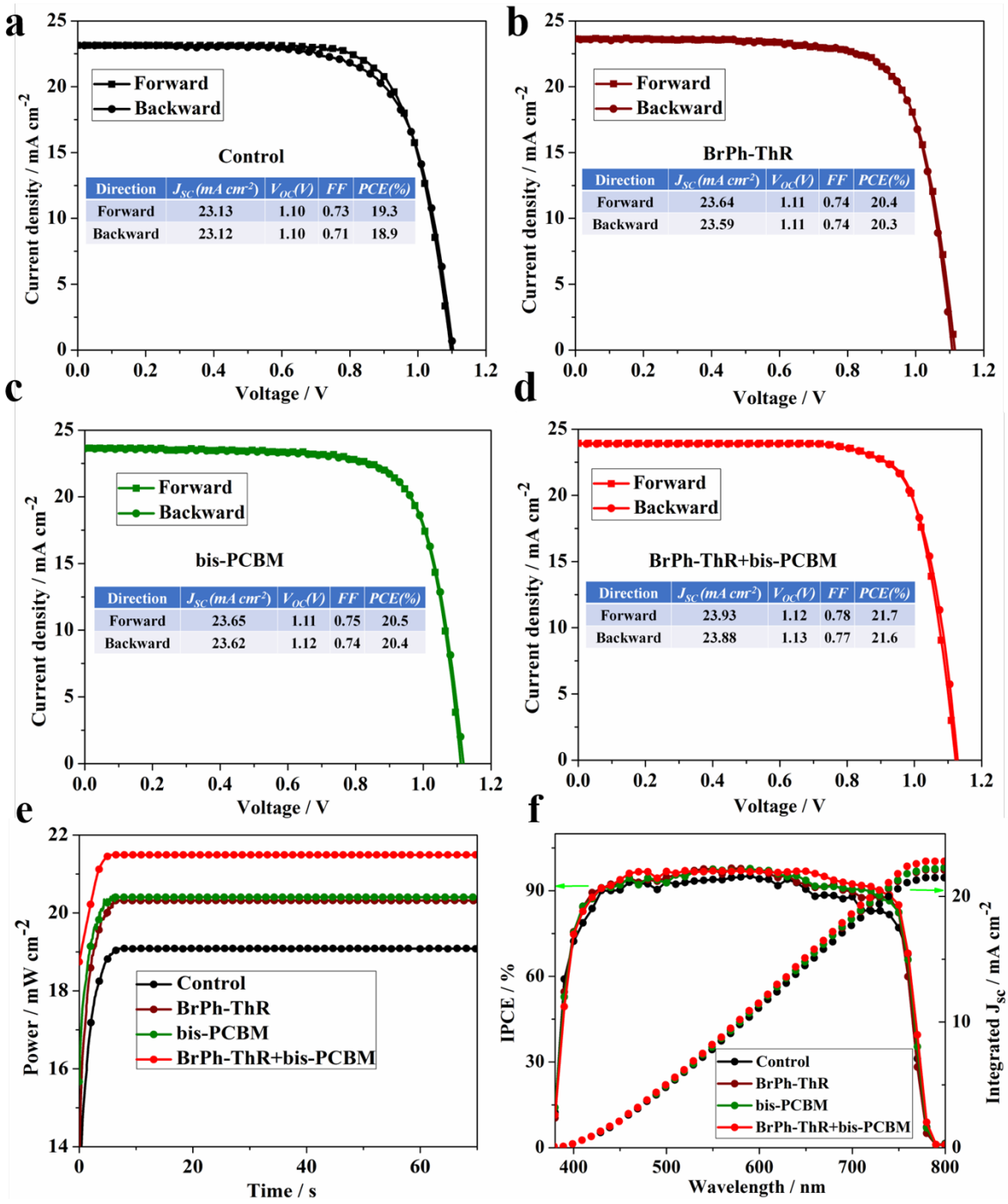

Figure 5 Current-voltage hysteresis curves of perovskite solar cells comprising champion devices measured starting with backward scan and continuing with forward scan with a bias step of 5 mV .a)control; b) BrPh-ThR; c) bis-PCBM;d) BrPh-ThR+ bis-PCBM. e) The stabilized power output of the corresponding devices. f) IPCE spectra and integrated current curves of the corresponding devices.

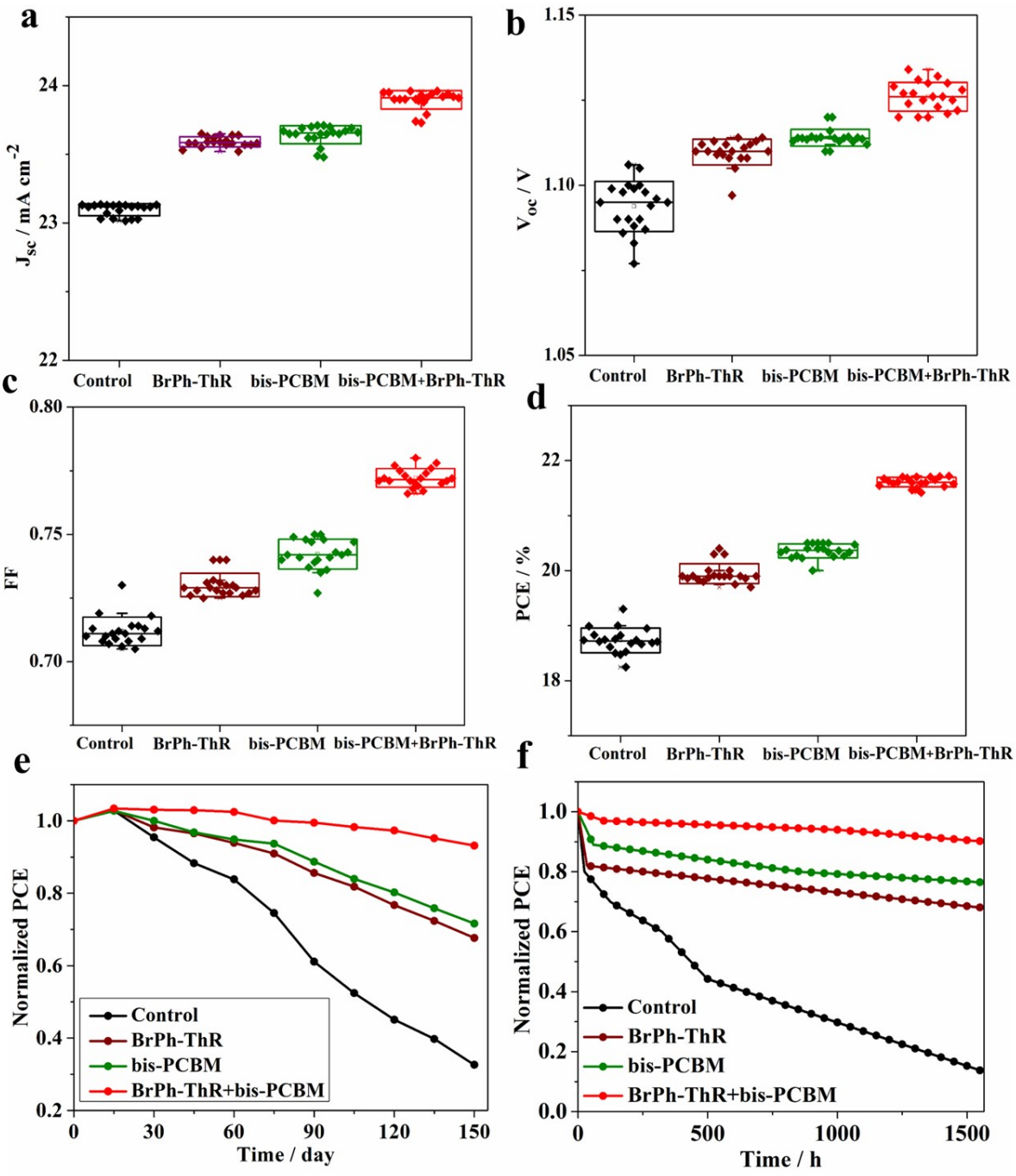

Figure 6 Photovoltaic metrics of devices based on corresponding perovskite layers. a)*Jsc* ; b) *Voc* ; c)FF; d) PCE; e) The stability of corresponding perovskite solar cells in ambient environment of 10-20% relatively humidity dark storage without any encapsulation at room temperature. f) The stability of corresponding perovskite solar cells under continuous full sun illumination and maximum power point tracking in a nitrogen atmosphere at room temperature.